Available online at www.sciencedirect.com

SCIENCE DIRECT®

Journal of Applied Geophysics 57 (2005) 179–191

JOURNAL OF APPLIED GEOPHYSICS

www.elsevier.com/locate/jappgeo

Vertical radar profiling: influence of survey geometry on first-arrival traveltimes and amplitudes

Jens Tronicke*, Michael D. Knoll

Center for Geophysical Investigation of the Shallow Subsurface, Boise State University, Boise, ID 83725, USA

Received 3 September 2003; accepted 11 November 2004

Abstract

In vertical radar profiling (VRP), the receiver antenna is located within a borehole while the transmitter antenna is placed at varying offsets from the borehole. VRP surveys are primarily used to reconstruct subsurface georadar velocities by inverting direct-wave traveltimes. We examine the VRP technique and associated concepts that need to be considered when acquiring, analyzing and interpreting VRP data. Using simple ray-based models, we investigate the occurrence of waves critically refracted at the earth's surface for common near-surface velocity distributions and acquisition geometries. Our analysis demonstrates that these refracted waves are major limiting factors in VRP surveying. They interfere with the direct arrivals and hence reduce the reliability of direct-arrival traveltimes and amplitudes. To avoid waves critically refracted at the earth's surface in the recorded data, near-offset transmitter locations are preferred. We also analyze the amplitude sensitivity of the VRP antenna configuration, which is represented by an infinitesimal horizontal dipole located at the interface between two half-spaces and an infinitesimal vertical dipole in full-space. By combining the far-field radiation patterns of these two dipoles, we determine transmitter–receiver combinations for which maximum sensitivity is expected. A key result is that medium to far offsets between the transmitter and the borehole provide the highest amplitude signals. As a consequence, there is a natural trade-off between the requirement to avoid waves critically refracted at the earth's surface and the quest to record high-amplitude data. Finally, we apply the developed concepts in analyzing a multi-offset VRP field data example. This field data example illustrates how multiple offsets between the transmitter antenna and the borehole allow high-quality data to be measured over a large depth range.

Keywords: Georadar; Vertical radar profiling; Traveltime modeling; Radiation pattern; Survey design

1. Introduction

Borehole georadar techniques are increasingly used for probing the shallow subsurface in engineering and environmental applications. Commonly

* Corresponding author. Present address: Swiss Federal Institute of Technology, Institute of Geophysics, ETH-Hönggerberg, CH-8093 Zürich, Switzerland. Tel.: +41 1 633 2727; fax: +41 1 633 1065.

E-mail address: jens@aug.ig.erdw.ethz.ch (J. Tronicke).

0926-9851/$ - see front matter © 2004 Elsevier B.V. All rights reserved.
doi:10.1016/j.jappgeo.2004.11.001

applied techniques include crosshole surveying (e.g., Olsson et al., 1992; Binley et al., 2001; Tronicke et al., 2001) and single-hole reflection surveying (e.g., Olsson et al., 1992, Lane et al., 1998; Hollender et al., 1999). In crosshole surveying, transmitter and receiver antennas are placed in two different boreholes and a transmission experiment is performed. By inverting the arrival times or amplitudes of first arrivals, an image of electromagnetic wave velocity or attenuation for the inter-borehole plane is determined. In single-hole reflection surveying, the two antennas are located in the same borehole and reflected arrivals are analyzed using methods developed for surface-based reflection data.

Vertical radar profiling (VRP) is a rather new technique in which the receiving antenna is lowered down a borehole and the transmitting antenna is placed on the surface at one or more offsets from the borehole. VRP studies for characterization of the shallow subsurface have been published for hydrological (Knoll, 1996; Knoll and Clement, 1999; Tronicke et al., 2000; Buursink et al., 2002) and archaeological (Lu et al., 1996; Zhou and Sato, 2000) applications. These studies indicate that the VRP method is a promising shallow exploration tool that may replace or complement surface and crosshole georadar surveying. Electromagnetic velocity information can be determined from inversions of the direct arrival times (e.g., Knoll and Clement, 1999), and reflected or diffracted energy can be used to image subsurface structures (Zhou and Sato, 2000; Witten and Lane, 2003). Furthermore, VRP data can supplement crosshole georadar data sets by increasing the effective maximum aperture of the observations (e.g., Hammon et al., 2002).

VRP surveying is similar to the well-established vertical seismic profiling (VSP) technique (e.g., Hardage, 2000). In near-surface applications, VSP surveys are mainly used to construct subsurface velocity models and reflection images which can be used as a complement to surface seismic data (e.g., Jarvis and Knight, 2000) or as a link to important engineering or environmental parameters (e.g., Milligan et al., 1997; Moret et al., 2004). However, there are some significant differences between VRP and VSP surveys that need to be considered in VRP data analysis and interpretation. For example, radar velocities usually decrease from the surface through the vadose zone to the water-saturated zone, whereas seismic velocities generally increase. Because subsurface velocities affect all wave phenomena, the pattern of VRP arrivals may be quite different from the pattern of VSP arrivals recorded at the same location. Before adapting VSP processing and interpretation schemes to VRP data, we need to understand better the nature of electromagnetic wave propagation for typical VRP survey geometries.

In surface and downhole georadar surveys, the antenna radiation patterns strongly influence the amplitudes of the sampled wave fields. The directivity of the antennas depends on the electrical properties of the surrounding media. Numerous studies have been concerned with the radiation pattern of surface or downhole dipole antennas (e.g., Engheta et al., 1982; Sato and Thierbach, 1991; Arcone, 1995; Holliger et al., 2001; Lampe et al., 2003), but for the acquisition and interpretation of VRP data, the combination of a horizontal surface and a vertical downhole dipole antenna has to be considered. To the best of our knowledge, there have been no previous investigations of this antenna configuration and its influence on the amplitudes of recorded VRP data. The goal of the present study is to address the following three questions:

- How do waves critically refracted at the earth's surface influence VRP data and their interpretation?
- How does the specific VRP antenna configuration affect the recorded signals?
- Is there an optimal acquisition scheme for VRP data?

We begin by investigating the occurrence of arrivals critically refracted at the ground–air interface. To examine this issue, we compute the critical offsets x_c from the wellhead for different layered velocity distributions using a ray-approximation of electromagnetic wave propagation; that is, for given transmitting and receiving antenna positions, we compute the minimum distance from the borehole at which critical refraction wave propagation first occurs. For example, identifying and eliminating traveltimes from arrivals critically refracted at the

earth's surface might improve and stabilize results of first-arrival traveltime inversion using standard inversion schemes.

We then analyze the amplitude sensitivity of the VRP antenna configuration and its influence on the recorded data. To address this issue, we introduce a simple method for combining surface and downhole radiation patterns and compare our analytical results to those predicted by full waveform finite-difference modeling. The analysis of critically refracted arrivals and antenna radiation pattern effects allows us to draw some conclusions about how VRP data should be acquired and analyzed. Finally, we illustrate by means of a multi-offset field example how an understanding of critically refracted waves and radiation pattern effects can be helpful in processing and interpreting VRP field data. An important conclusion of our investigation is that there is a trade-off between the need to have short transmitter-borehole offsets to avoid the recording of critically refracted waves and the desire to have long transmitter-borehole offsets to avoid nulls in the radiation patterns. In this way, this paper investigates the influence of VRP survey geometry on first-arrival traveltimes and amplitudes, and serves as a tutorial on how to plan and execute a multi-offset VRP survey.

2. Identifying direct and critically refracted arrivals

Fig. 1 illustrates travelpaths and traveltime curves of major arrivals commonly observed in VRP experiments. The model in this figure comprises air with a georadar velocity c (0.3 m/ns) overlying successively a homogenous isotropic layer with velocity v_1 and thickness z_1 and a homogeneous isotropic half-space with velocity v_2. While the transmitter antenna is maintained at a fixed horizontal distance x_a from the borehole, the receiver antenna is lowered down the borehole at progressively increasing depths z_a. After the receiver antenna has been moved down the length of the borehole, the trans-

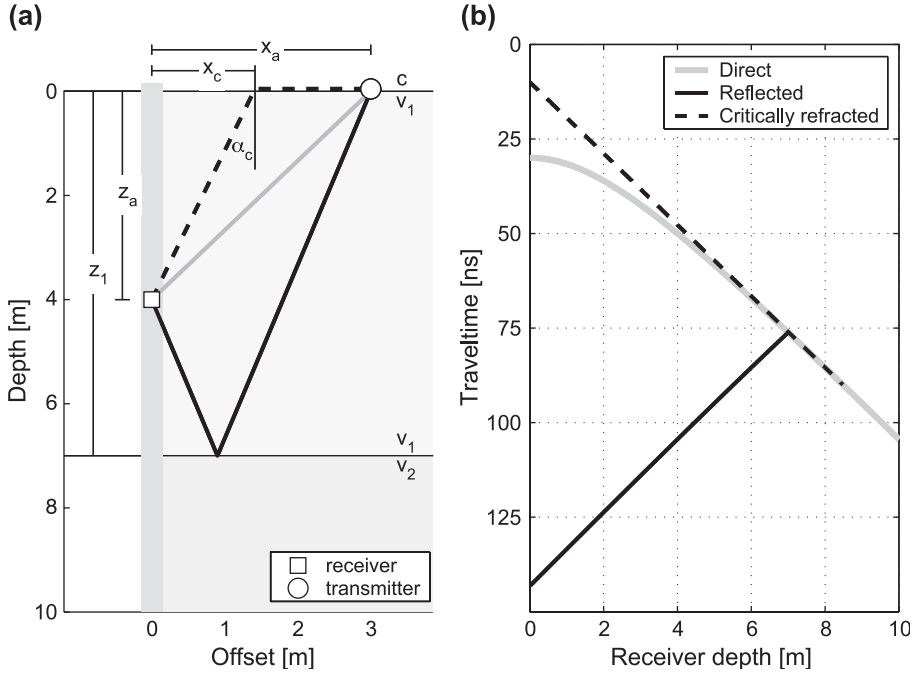

Fig. 1. For a fixed surface transmitter: (a) sketch illustrating VRP geometry and major travelpaths, and (b) corresponding traveltime curves. In (a), α_c is the critical angle at the ground–air interface defined by $\sin \alpha_c = v_1/c$, where c and v_1 are radar-wave velocities in air and in the shallow subsurface. v_2 is the radar-wave velocity below the subsurface reflecting interface. Both the travelpaths in (a) and the traveltime curves in (b) are calculated assuming a constant subsurface velocity of 0.1 m/ns and a horizontal reflecting interface at 7.0 m depth.

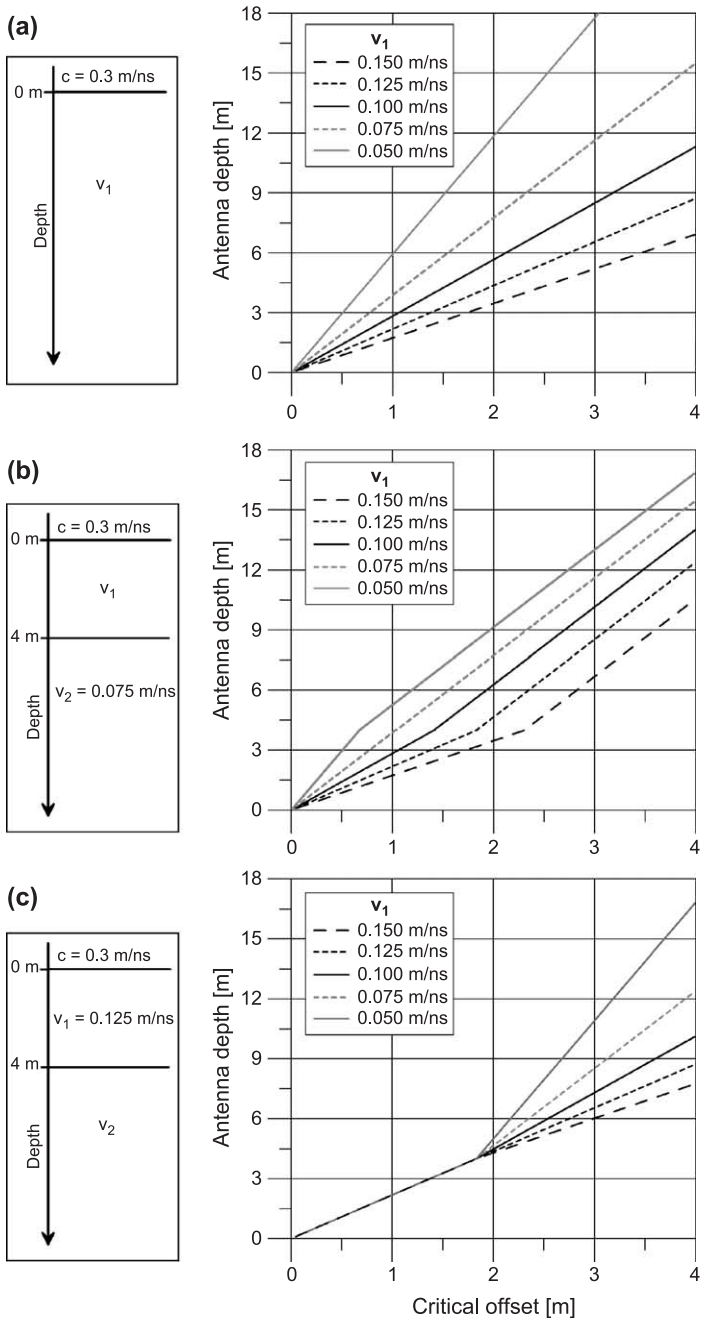

Fig. 2. Critical offset from borehole as a function of receiver-antenna depth for three suites of three-layer models: (a) air and homogeneous layer with thickness >18 m and a homogeneous half-space (latter not shown in model sketch); (b) air, 4.0-m-thick layer with variable velocity and a homogeneous half-space with a 0.075 m/ns constant velocity; (c) air, 4.0-m-thick layer with constant 0.125 m/ns velocity, and a homogeneous half-space with variable velocity.

mitter may be moved to a new location and the process repeated. Using geometrical optics as a high-frequency approximation of electromagnetic wave propagation, the traveltimes for the direct wave (t_{dir}), reflected wave (t_{ref}) and waves critically refracted at the earth's surface (t_{cri}) are given by:

$$t_{dir} = \frac{\sqrt{x_a^2 + z_a^2}}{v_1} \quad (1)$$

$$t_{ref} = \frac{\sqrt{x_a^2 + (2z_1 - z_a)^2}}{v_1} \quad (2)$$

$$t_{cri} = \frac{x_a}{c} + z_a\sqrt{\frac{1}{v_1^2} - \frac{1}{c^2}}. \quad (3)$$

The downgoing direct wave exhibits positive moveout (Eq. (1)), such that traveltimes increase as the recording depth increases, whereas the traveltimes of the upgoing reflections (Eq. (2)) decrease as the recording depth increases. In contrast to VSP surveys, waves critically refracted at the ground–air interface are often present in VRP data. Traveltimes of these waves increase linearly with receiver antenna depth (Eq. (3)). For short transmitter-borehole offsets and shallow receiver positions, critically refracted waves may interfere with the direct arrivals. This may complicate the determination of direct arrival times which are required for generating reliable subsurface velocity models. The point x_c along the surface from which the critically refracted wave propagates to a given depth z_a is given by:

$$x_c = z_a \cdot \tan\left(\arcsin\frac{v_1}{c}\right), \text{ for } z_a \leq z_1, \quad (4)$$

$$x_c = z_1 \cdot \tan\left(\arcsin\frac{v_1}{c}\right) + (z_a - z_1) \cdot \tan(\arcsin\frac{v_2}{c}), \text{ for } z_a > z_1. \quad (5)$$

Fig. 2 shows these critical offsets for three different suites of three-layer models selected to represent a wide variety of near-surface conditions. In Fig. 2a, the depth to the base of the first subsurface layer is beyond the maximum receiver antenna depth, so it is effectively a two-layer model. The critical offset increases uniformly with decreasing velocity contrast between air and the subsurface medium and with increasing antenna depth. The situation for a 4-m-thick subsurface layer with different velocities overlying a homogeneous half-space with fixed velocity is presented in Fig. 2b. This model includes the case of a vadose zone overlying a water-saturated zone. Until the receiver antenna reaches the depth of the interface, the results are the same as in Fig. 2a. Beyond 4 m depth, the slope changes significantly as a function of the velocity contrast between the two subsurface layers. Fig. 2c is based on a similar model to that of Fig. 2b, except the velocity of the upper subsurface layer is fixed and the velocity of the lower one is varied. Again, at antenna depths below the interface, the critical offset x_c depends significantly on the contrast in subsurface velocities.

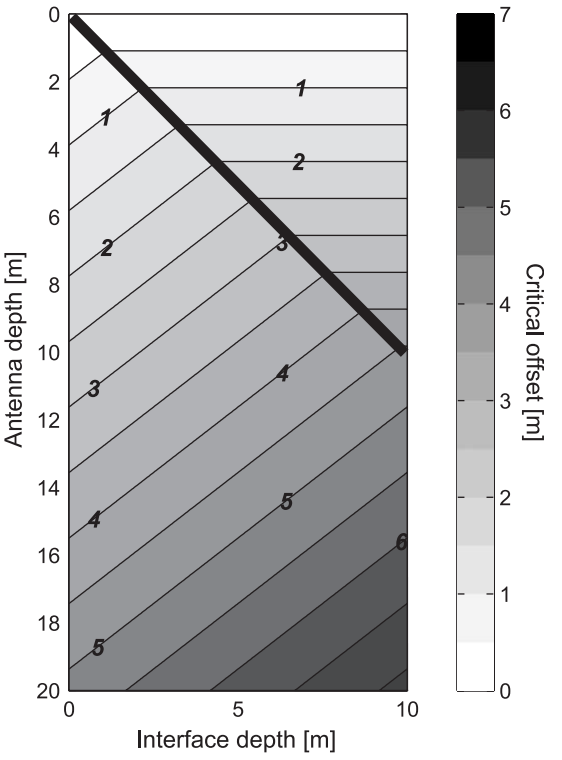

Fig. 3. Critical offset from borehole as a function of receiver-antenna and interface depths for a three layer case: c=0.3 m/ns (air), v_1=0.125 m/ns and v_2=0.075 m/ns. The black line separates antenna positions above the interface from those below.

Fig. 3 illustrates x_c as a function of receiver antenna and interface depth assuming a fixed three-layer velocity model: c=0.3 m/ns, v_1=0.125 m/ns and v_2=0.075 m/ns. The interface depth influences strongly x_c, such that the deeper the interface, the larger x_c is for a given receiver-antenna depth. All

model results shown in Figs. 2 and 3 demonstrate that arrivals critically refracted at the earth's surface are likely to occur in shallow VRP surveys for borehole depths around 10 to 20 m. For locations at which subsurface velocities are approximately known, our modeling procedure and results allow investigators to estimate transmitter-borehole offsets that avoid unwanted critically refracted arrivals. Furthermore, such plots help to identify critically refracted waves during data processing and interpretation.

3. Effects of radiation patterns on recorded amplitudes

Commercially available georadar surface and borehole antennas are usually half-wave dipole antennas with strong directional radiation patterns that depend on the electrical properties of the surrounding media. Commonly, a surface dipole antenna is approximated by a horizontal infinitesimal electric dipole located at the interface between two homogeneous half-spaces, one representing air with dielectric permittivity ε_0 and one representing the subsurface with dielectric permittivity $\varepsilon_r\varepsilon_0$, where ε_r is the relative permittivity of the medium (Engheta et al., 1982). The associated dipole patterns depend strongly on the contrast in dielectric permittivities between the upper and lower half-spaces. Although recent studies (e.g., Holliger and Bergmann, 1998; van der Kruk and Slob, 2000; Lampe et al., 2003) show that the characteristics of this model may diverge from those of realistic georadar surface antennas, the infinitesimal dipole model describes the main directional dependence of E-field values associated with a dipole antenna located on the surface. For a dipole antenna located within an air-filled borehole, Holliger et al. (2001) find that the radiation pattern of a vertical infinitesimal dipole in full-space is a valid approximation. When the borehole contains water, the radiation pattern is distorted, such that this approximation may be inadequate (Holliger et al., 2001).

Here, we focus on the angular E-field amplitude trends that are expected in a VRP survey. Typically, the dipole axes of the transmitting and receiving antenna are oriented perpendicular to each other (Fig. 4; horizontal at the surface and vertical in the borehole). We only consider the case for which the two dipole axes are located in the same plane (copolarized orientation of the antennas). In investigating the amplitude sensitivity of this antenna configuration, we apply the often used far-field approximation for the surface antenna (Engheta et al., 1982) and the full-space approximation for the borehole antenna (Holliger et al., 2001). For a lower medium with dielectric permittivity of $5\varepsilon_0$, the radiation patterns of the surface and borehole dipoles, normalized to their individual maximum values, are shown in Fig. 5a and b. Because we consider copolarized antennas, only the E-plane (vertical plane containing the antenna elements) of the surface dipole needs to be considered.

In Fig. 5a, the far-field radiation pattern of the surface antenna (gray curve) has a three-lobed structure in the subsurface with distinct nulls at 0°, 180°, 243° and 297°. For comparison, we show on the same figure the equivalent finite-difference modeled radiation pattern (black curve) for a finite-length surface antenna (after Lampe et al., 2003). The general shape of the numerical radiation pattern is comparable to the analytical far-field approximation, except the side lobes are less pronounced and the nulls are replaced by low sensitivities.

The radiation pattern of the borehole antenna (Fig. 5b) calculated using the far-field approximation of a vertical dipole in full-space is characterized by a cosine function with nulls at 90° and 270°. When comparing Fig. 5a with Fig. 5b, significant differences

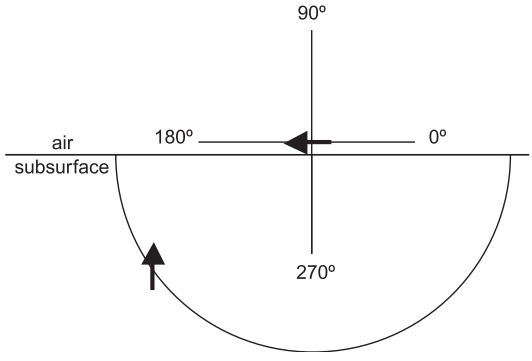

Fig. 4. Sketch illustrating antenna layout in a typical VRP experiment. The horizontal surface dipole antenna is represented by the horizontal arrow and the vertical borehole dipole by the vertical arrow.

in angular sensitivity between the horizontal and vertical dipoles are clearly visible.

Fig. 5c shows the results of combining the borehole dipole radiation pattern with the vertical components of the surface dipole radiation patterns via simple multiplication. This is common practice for describing a two-antenna system (Arcone, 1995). The light gray curve in Fig. 5c represents the result of multiplying together the two approximations whereas the black points represent the numerical radiation pattern extracted from finite-difference modeling by considering only the z-component of the E-field. The general shape of the two radiation patterns plotted in Fig. 5c is quite similar, showing that our simple analytical model describes the main characteristics of amplitude sensitivities associated with the copolarized VRP antenna configuration. We should not, however, include the sharp nulls (except for that at 270°) and second-order maxima (e.g., those at ~240° and ~300°) in our analysis and interpretation.

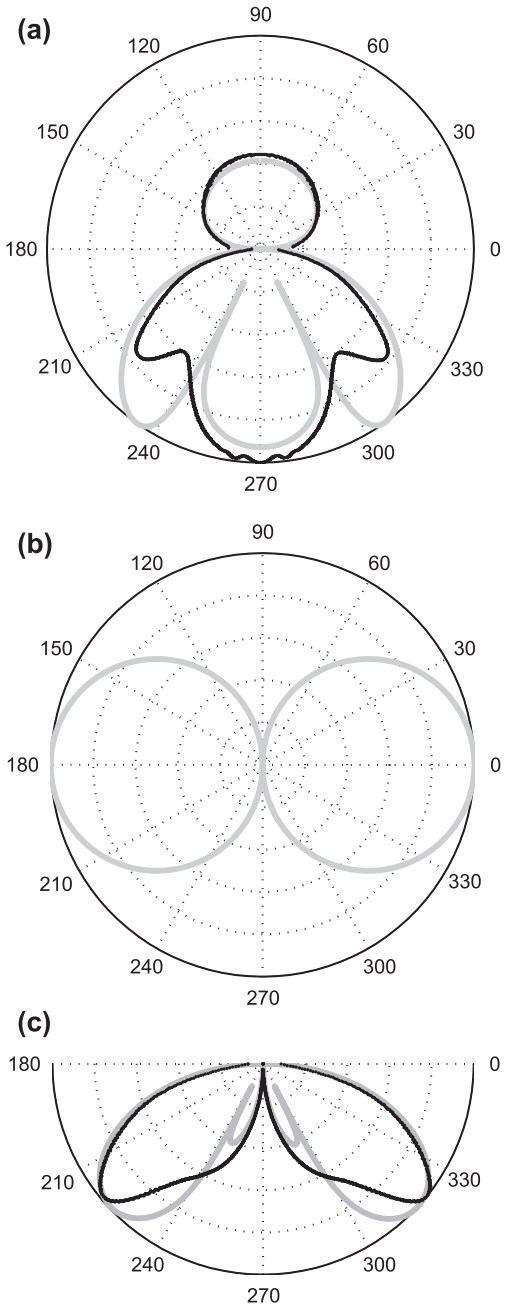

Fig. 5. (a) Far-field approximated (gray) and finite-difference modeled (black) radiation patterns (in E-plane) for a horizontal infinitesimal dipole located on a dielectric half-space; (b) Far-field approximated radiation pattern for a vertical infinitesimal dipole within a full-space; (c) Far-field approximated (gray) and finite-difference modeled (black) radiation patterns for a copolarized VRP antenna configuration (see Fig. 4). In (a) and (b), the dielectric permittivity of the lower half-space is $5\varepsilon_0$. Each curve is normalized to its individual maximum value. For angle definition, see Fig. 4.

Fig. 6 shows combinations of the analytical surface and borehole dipole radiation patterns for different subsurface dielectric permittivities. The subsurface permittivities vary between $1\varepsilon_0$ and $16\varepsilon_0$, spanning values typical of many near-surface materials. Since we are only interested in relative changes, all patterns are normalized with respect to their individual maximum value. The plots in Fig. 6 show strong directivities, with low sensitivities in the directions of both dipole axes. For subsurface permittivities of $4\varepsilon_0$, $9\varepsilon_0$ and $16\varepsilon_0$, the widths of the main lobes increase with increasing dielectric permittivity, approaching the pattern for a subsurface permittivity of $1\varepsilon_0$ (i.e., for a homogenous full space). Maximum sensitivities for all shown models occur at ~225° and ~315°. The general shapes of the curves are very similar, indicating that the influence of the medium beneath and surrounding the antennas is not as pronounced in VRP data as it is in surface data.

Both the investigation of arrivals critically refracted at the earth's surface and the study of amplitude sensitivity illustrate the influence of acquisition geometry on VRP data. We have learned that critically refracted arrivals are likely to be recorded and that amplitude sensitivity depends strongly on the

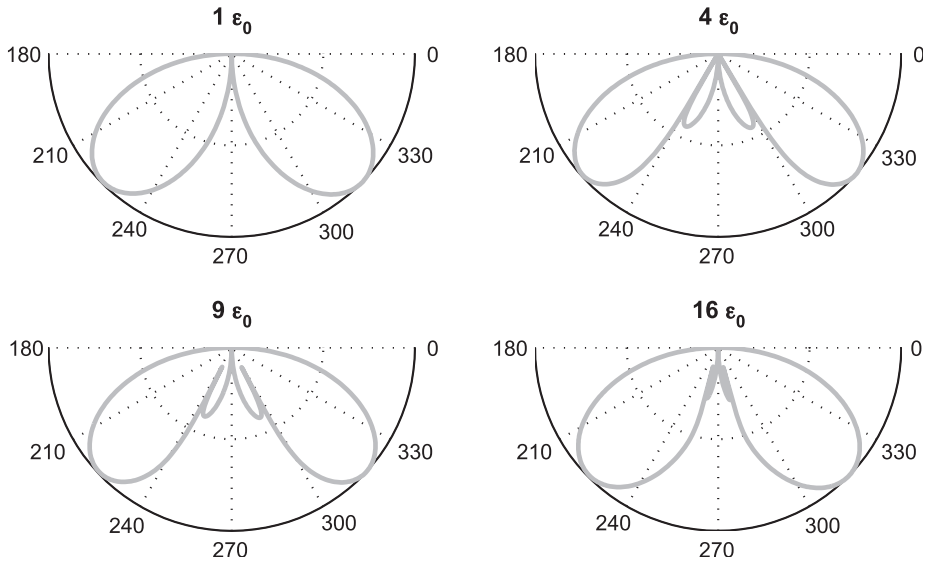

Fig. 6. Influence of subsurface dielectric permittivity on the amplitude sensitivity of the VRP antenna configuration. Radiation patterns are the result of combining the analytical far-field radiation patterns of an infinitesimal horizontal dipole with that of an infinitesimal vertical dipole. Different diagrams represent different subsurface dielectric permittivities (values shown above each plot). Each curve is normalized to its individual maximum value. For angle definition, see Fig. 4.

angle between the surface and the borehole antenna. In the next section, we demonstrate how these issues manifest themselves in field data.

4. Field data example

In 1998, a multi-offset VRP data set was recorded in well A1 at the Boise Hydrogeophysical Research Site (BHRS). The BHRS is a research wellfield located on a gravel bar of the Boise River where much is known about the subsurface distribution of hydrologic and geophysical properties (Barrash and Knoll, 1998; Barrash et al., 1999; Knoll and Clement, 1999; Peretti et al., 1999; Peterson et al., 1999; Barrash and Clemo, 2002). Well A1 penetrates ~20 m of coarse alluvial sediments that have been subdivided into five units with varying amounts of cobble and sand and different porosity geostatistics (Barrash and Clemo, 2002). The groundwater table during the experiments was located 2.55 m below land surface.

A commercial georadar system (Mala RAMAC/GPR) with 250-MHz borehole antennas was used to acquire the VRP data. The antennas were resistively loaded electric-field dipoles with integral batteries and transmitter and receiver electronics. Fiber-optic cables were used to transfer timing information and digital data between the antennas and the radar control unit. The receiver station spacing in each transmitter gather was 0.05 m. In total, six common-transmitter gathers were recorded over a 1.0–6.0 m transmitter-borehole offset range (step size 1.0 m along the surface).

Fig. 7 shows two common-transmitter gathers recorded while the transmitter was positioned 3.0 and 6.0 m from the borehole. The only processing applied to these gathers is zero-time correction, DC shift removal and application of the same depth-dependent scaling function that preserves relative amplitude information. On both gathers, the slope of the first arrivals shows a significant change at ~2.5 m depth and minor fluctuations at deeper levels. This change in slope is related to the 2.55-m groundwater table depth. Some secondary arrivals are clearly visible (e.g., above the groundwater table between ~40 and ~80 ns). For receiver positions above 2.5 m, interference of different events, including the direct arrivals, complicates their identification. To identify the complicated interfering events in the vadose zone and the direct-traveling energy in the saturated zone, a

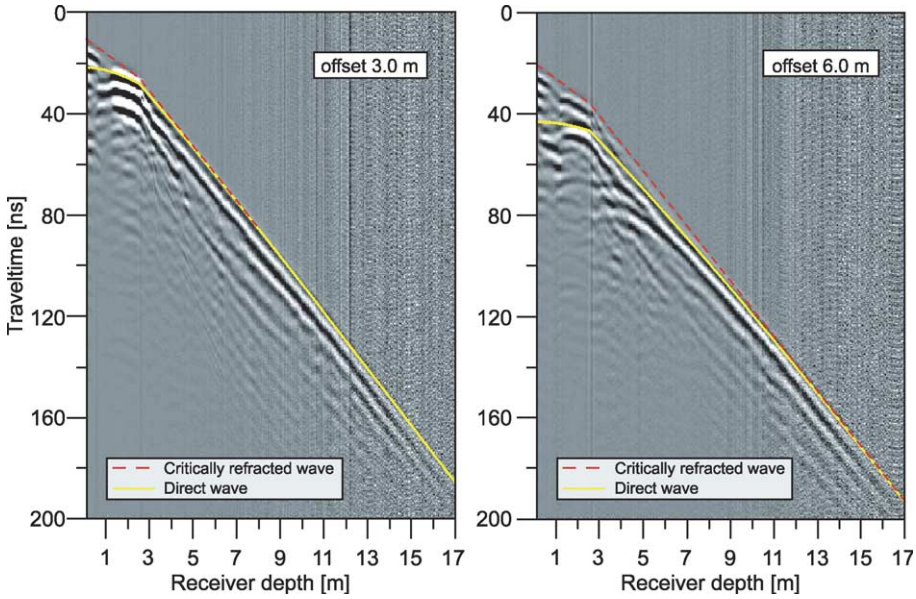

Fig. 7. Two common transmitter gathers of the BHRS data set recorded at different borehole offsets. The two gathers are displayed with the same depth-scaled gain. Overlain curves show arrival times for the critically refracted waves (dashed red curves) and for the direct waves (solid yellow curves) calculated using a simplified model consisting of air (c=0.3 m/ns), a 2.55-m-thick homogenous layer (v_1=0.14 m/ns) and a homogenous half-space (v_2=0.09 m/ns).

more detailed analysis based on the concepts developed above is necessary.

As a first approximation, the radar stratigraphy at the BHRS can be modeled as a horizontally layered earth consisting of three layers (air, unsaturated sediments and saturated sediments). To ensure accurate and independent estimates of subsurface georadar velocities for further analysis, we use information extracted from complementary surface and crosshole georadar data recorded at the BHRS (Peretti et al., 1999; Peterson et al., 1999; Tronicke et al., 2004). The ground wave observed in a nearby CMP data set yields a velocity of 0.14 m/ns for the upper part of the vadose zone. Analysis of crosswell tomographic data yields an average velocity of 0.09 m/ns for the saturated zone. By using this simple velocity model, we can estimate the arrival times of direct waves and waves critically refracted at the earth's surface using a ray-tracing algorithm and Eqs. (4) and (5) (red and yellow lines in Fig. 7). For the 3.0-m offset gather in Fig. 7, critically refracted waves should be present down to receiver depths of ~7.8 m, and for the 6.0-m offset gather, critically refracted waves should be present for all receiver positions. In neither transmitter gather are the critically refracted and direct arrivals clearly separable, because their traveltimes are so similar and the finite length of the wavelets further complicates the analysis.

We now analyze amplitude variations as functions of transmitter offset and receiver depth. We analyze the data without applying any kind of manipulation because we are interested in the influence of survey geometry on signal-to-noise ratios and want to insure that results are not biased by spherical divergence and/or attenuation compensations. To insure that any residual DC bias does not contaminate the results, we pick peak-to-peak amplitudes of the first arriving wavelet. In Fig. 8a, picked amplitudes for all six transmitter gathers are plotted as functions of receiver depth. The overall shapes of the curves are similar for all offsets. In the vadose zone above 2.55 m, strong variations are observed, whereas in the saturated zone, all curves show steadily decreasing amplitudes with only minor variations. Although the relatively minor fluctuations are comparable at different offsets (e.g., at receiver depths of ~10 m, five of the six curves show relative minima followed by slight increases in amplitude), there are significant differences in the

absolute values of the amplitudes (note the log scale of Fig. 8). Because of rapidly decreasing signal strength, amplitudes in the nearest offset gathers (transmitter-borehole offsets of 1.0 and 2.0 m) could only be picked down to receiver depths of ~10 and ~12 m, respectively. In contrast, strong signals in the gathers recorded at longer offsets allowed amplitudes to be picked down to depths of ~14 to ~16 m.

Other trends are visible in the amplitude plots. In particular, the decay of amplitude with receiver depth varies with transmitter offset; at shallow receiver positions (e.g., 3–4 m), the highest amplitudes are observed at the near-offset transmitter gathers, whereas at deeper receiver positions (e.g., 9–10 m), the opposite is seen. These amplitude variations are qualitatively consistent with our radiation-pattern analysis. For short transmitter-borehole offsets, the direct ray paths become steeper as the receiver depth increases, gradually approaching the vertical (around 270° in Figs. 5 and 6). Consequently, relatively long transmitter-borehole offsets would appear to be desirable. In contrast to this argument, we know that far-offset gathers are more contaminated with critically refracted waves than near-offset ones (i.e., increasing the offset increases the range of receiver depths over which critically refracted waves are recorded). Both of these effects (the occurrence of critically refracted waves and large amplitude variations that result from the radiation patterns of dipole antennas) have to be considered when estimating intrinsic attenuation.

Using the simple three-layer velocity model given above, and Eqs. (4) and (5), we have identified and then excluded from analysis those transmitter–receiver pairs that are likely to have waves critically refracted at the earth's surface as the first arrivals (Fig. 8b). This procedure results in the elimination of large amounts of data (e.g., the entire

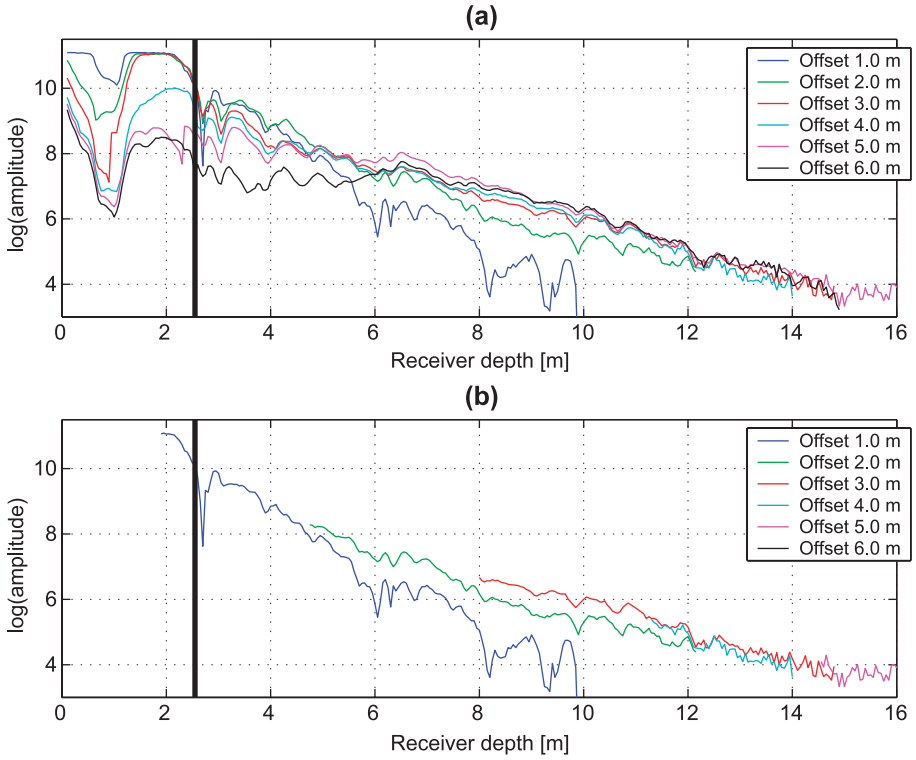

Fig. 8. First cycle amplitudes as a function of receiver depth for all measured transmitter offsets. In (a), all picked data are shown, whereas in (b), data are only plotted for depths where no critically refracted arrivals are expected. The thick solid lines at a depth of 2.55 m represent groundwater table depth. For details, see text.

transmitter gathers recorded at the two largest offsets). Fortunately, the three near-offset transmitter gathers provide complementary information at depths of 2–16 m, thus ensuring optimal data quality over all depth ranges.

A companion analysis of the traveltime data is carried out to illustrate the effect that arrivals critically refracted at earth's surface can have on velocity models generated using VRP traveltime data; that is, we invert the multi-offset VRP traveltime data with and without suspected critical refractions and compare the results. The traveltime data with critically refracted first arrivals correspond to the data in Fig. 8a, and the data without critically refracted arrivals correspond to the edited data in Fig. 8b. For inversion, we used a standard 1-D iterative inversion scheme which uses curved rays (Maurer et al., 1999) and parameterized the subsurface into two homogeneous velocity layers, representing the vadose zone and the saturated zone, respectively. The boundary between these two zones is located at 2.55 m depth to reflect the depth of the water table at the time of the VRP survey.

The results of the two traveltime inversions are shown in Fig. 9. Using the entire traveltime data set (with critically refracted arrivals), the velocities of the vadose zone and saturated zone are 0.16 and 0.087 m/ns, respectively. For the edited data set, these velocities are 0.133 and 0.092 m/ns which are much closer to the values obtained from analysis of CMP and crosswell georadar data from the site. In addition, the root-mean-square (RMS) residual which characterizes the goodness of fit of the predicted traveltime data illustrates the benefit of using the edited data set. Removing the suspected critically refracted first arrivals from the traveltime data results in a threefold decrease in the RMS residual and a concomitant increase in the reliability and accuracy of the corresponding velocity model.

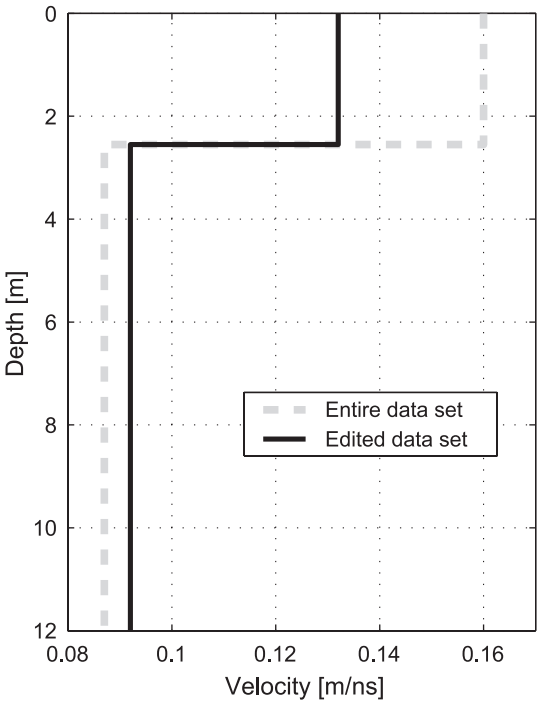

Fig. 9. Inverted two-layer velocity model using the entire traveltime data set (RMS residual 2.76 ns) compared to one using the data set in which potential critically refracted arrivals are eliminated in analogy to Fig. 8b (edited data set, RMS residual 0.84 ns).

5. Concluding discussion

Using a simple ray-based model, we have shown for a variety of commonly observed velocity distributions that unwanted waves critically refracted at the earth's surface may significantly influence VRP data. Their presence reduces the reliability of direct-arrival traveltimes and amplitudes, limiting the accuracy of derived subsurface velocity and attenuation models. We suggest that the identification of these critically refracted arrivals is a key requirement in VRP data acquisition, processing and interpretation.

Another important factor is the angular sensitivity of the antenna radiation patterns. We developed a simple analytical model by combining the far-field radiation pattern of a horizontal dipole located on the top of a half-space with the radiation pattern of a vertical dipole situated within a full-space. For different subsurface dielectric permittivities, our approximate model shows minimum amplitudes in the directions of both dipole axes and maximum values in directions oriented ~45° relative to these axes. Comparison of the far-field and finite-difference modeled radiation patterns demonstrates that the sharp minima in the former are regions of lower amplitude in the latter. As a result, the critical-angle

minima and second-order maxima are not as pronounced as shown in our model. Nevertheless, because the general shapes of the radiation patterns are well represented by the analytical far-field approximation, our simple model allows us to investigate the general angular amplitude sensitivity associated with typical VRP antenna configurations. Understanding this angular dependency helps to optimize VRP survey design needed for specific applications, such as direct arrival traveltime inversion or reflection imaging.

To avoid recording critically refracted waves requires relatively short transmitter-borehole offsets. Yet, the general amplitude sensitivity of the VRP antenna configuration suggests that near-vertical ray paths should be avoided, because of the low sensitivity of the vertical receiver dipole at such angles resulting in lower signal-to-noise ratios for the corresponding data. This requires that the transmitter-borehole offset be relatively large. As a consequence, for a single-offset VRP experiment, a compromise has to be found between suppressing critically refracted waves (near-offset transmitter locations preferred) and recording data with sufficiently high signal-to-noise ratios (medium- to far-offset transmitter locations preferred). Depending on the specific site conditions, the signal-to-noise ratios at large offsets may also be negatively influenced by intrinsic attenuation.

Our analysis of a multi-offset VRP field data set illustrated the need to understand the characteristics of the first arriving energy. Having access to data recorded with multiple transmitter-borehole offsets proved to be extremely useful for extracting high-quality data over a large depth range. As a result of our synthetic and field studies, we recommend that VRP data be collected using multiple transmitter-borehole offsets to ensure maximum data quality.

Acknowledgements

The first author acknowledges financial support by the German Science Foundation (DFG) sponsoring a research fellowship at CGISS, Boise State University, Idaho, where most of the presented work has been carried out. The second author acknowledges funding from the Army Research Office, Grant DAAG55-98-1-0277. We thank Albane Saintenoy for help acquiring the multi-offset VRP data from the BHRS, Bernhard Lampe for carrying out the finite-difference modeling of the radiation patterns and Alan G. Green for fruitful comments and suggestions. Comments by Editor-in-chief James W. Rector and two anonymous journal reviewers greatly improved the quality of this manuscript.

References

Arcone, S.A., 1995. Numerical studies of the radiation patterns of resistively loaded dipoles. J. Appl. Geophys. 33 (1–3), 39–52.

Barrash, W., Clemo, T., 2002. Hierarchical geostatistics and multifacies systems: Boise Hydrogeophysical Research Site, Boise, Idaho. Water Resour. Res. 38, 1196.

Barrash, W., Knoll, M.D., 1998. Design of research wellfield for calibrating geophysical methods against hydrologic parameters. Proceedings of the 1998 Conference on Hazardous Waste Research, May 18–21, 1998, Snowbird, UT, Great Plains/Rocky Mountains Hazardous Substance Research Center, Kansas State University, pp. 296–318.

Barrash, W., Clemo, T., Knoll, M.D., 1999. Boise Hydrogeophysical Research Site (BHRS): objectives, design, initial geostatistical results. Proceedings, Symposium on the Application of Geophysics to Engineering and Environmental Problems, 14–18 March 1999, Oakland, California. Engineering and Environmental Geophysical Society, pp. 389–398.

Binley, A., Winship, P., Middleton, R., Pokar, M., West, J., 2001. High-resolution characterization of vadose zone dynamics using cross-borehole radar. Water Resour. Res. 37, 2639–2652.

Buursink, M.L., Lane, J.W., Clement, W.P., Knoll, M.D., 2002. Use of vertical-radar profiling to estimate porosity at two New England sites and comparison to neutron log porosity. Proceedings, Symposium on the Application of Geophysics to Engineering and Environmental Problems, 10–14 February 2002, Las Vegas, Nevada. Engineering and Environmental Geophysical Society. 15 pp.

Engheta, N., Papas, C.H., Elachi, C., 1982. Radiation patterns of interfacial dipole antennas. Radio Sci. 17, 1557–1566.

Hammon III, W.S., Zeng, X., Corbeanu, R.M., McMechan, G.A., 2002. Estimation of the spatial distribution of fluid permeability from surface and tomographic GPR data and core, with a 2-D example from the Ferron Sandstone, Utah. Geophysics 67, 1505–1515.

Hardage, B.A., 2000. Vertical Seismic Profiling, Principles. Handbook of Geophysical Exploration, Seismic Exploration. Pergamon. 552 pp.

Hollender, F., Tillard, S., Corin, L., 1999. Multifold borehole radar acquisition and processing. Geophys. Prospect. 47, 1077–1090.

Holliger, K., Bergmann, T., 1998. Accurate and efficient FDTD modeling of ground-penetrating radar antenna radiation. Geophys. Res. Lett. 25, 3883–3886.

Holliger, K., Musil, M., Maurer, H.R., 2001. Ray-based amplitude tomography for crosshole georadar data: a numerical assessment. J. Appl. Geophys. 47, 285–298.

Jarvis, K.D., Knight, R., 2000. Near-surface VSP surveys using the seismic cone penetrometer. Geophysics 65, 1048–1056.

Knoll, M.D., 1996.A petrophysical basis for ground penetrating radar and very early time electromagnetics: electrical properties of sand–clay mixtures. PhD dissertation, University of British Columbia, Vancouver, Canada, 318 pp.

Knoll, M.D., Clement, W.P., 1999. Vertical radar profiling to determine dielectric constant, water content and porosity values at well locations. Proceedings, Symposium on the Application of Geophysics to Engineering and Environmental Problems, 14–18 March 1999, Oakland, California. Engineering and Environmental Geophysical Society, pp. 821–830.

Lampe, B., Holliger, K., Green, A.G., 2003. A finite-difference time-domain simulation tool for ground-penetrating radar antennas. Geophysics 68, 971–987.

Lane, J.W., Haeni, F.P., Versteeg, R., 1998. Use of a multi-offset borehole-radar reflection method in fractured crystalline bedrock at Mirror Lake, Grafton County, New Hampshire. Proceedings, Symposium on the Application of Geophysics to Engineering and Environmental Problems, 22–26 March 1998, Chicago, IL. Engineering and Environmental Geophysical Society, pp. 359–368.

Lu, Y., Sato, M., Hiroaki, N., 1996. Application of GPR in archaeology using boreholes. 6th International Conference on Ground Penetrating Radar: Sendai, Japan, pp. 499–504.

Maurer, H.R., Van der Veen, M., Giudici, J., Springman, S., 1999. Determining elastic soil properties at small strains. Proceedings, Symposium on the Application of Geophysics to Engineering and Environmental Problems, 14–18 March 1998, Oakland, CA, pp. 417–424.

Milligan, P.A., Rector, J.W., Bainer, R.W., 1997. Hydrophone VSP imaging at a shallow site. Geophysics 62, 842–852.

Moret, G.J.M., Clement, W.P., Knoll, M.D., Barrash, W., 2004. VSP traveltime inversion: near-surface issues. Geophysics 69, 345–351.

Olsson, O., Falk, L., Forslund, O., Lundmark, L., Sandberg, E., 1992. Borehole radar applied to the characterization of hydraulically conductive fracture zones in crystalline rock. Geophys. Prospect. 40, 109–142.

Peretti, W.R., Knoll, M.D., Clement, W.P., Barrash, W., 1999. 3-D GPR imaging of complex fluvial stratigraphy at the Boise Hydrogeophysical Research Site. Proceedings, Symposium on the Application of Geophysics to Engineering and Environmental Problems, 14–18 March 1999, Oakland, CA. Engineering and Environmental Geophysical Society, pp. 555–564.

Peterson, J.E., Majer, E., Knoll, M.D., 1999. Hydrogeological property estimation using tomographic data at the Boise Hydrogeophysical Research Site. Proceedings, Symposium on the Application of Geophysics to Engineering and Environmental Problems, 14–18 March 1999, Oakland, CA. Engineering and Environmental Geophysical Society, pp. 629–638.

Sato, M., Thierbach, R., 1991. Analysis of a borehole radar in cross-hole mode. IEEE Trans. Geosci. Remote Sens. 29, 899–904.

Tronicke, J., Dietrich, P., Appel, E., 2000. Georadar velocity determination: a comparison of different techniques. Proceedings, Sixth Meeting of EEGS-ES: Bochum, Germany, GR01, 4 pp.

Tronicke, J., Tweeton, D.R., Dietrich, P., Appel, E., 2001. Improved crosshole radar tomography by using direct and reflected arrival times. J. Appl. Geophys. 47, 97–105.

Tronicke, J., Holliger, K., Barrash, W., Knoll, M.D., 2004. Multivariate analysis of cross-hole georadar velocity and attenuation tomograms for aquifer zonation. Water Resour. Res. 40, W01519, doi:10.1029/2003WR002031.

van der Kruk, J., Slob, E.C., 2000. The influence of the soil on reflections from above surface objects in GPR data. Proceedings, Eighth International Conference On Ground Penetrating Radar, Queensland, Australia, pp. 453–457.

Witten, A., Lane, J., 2003. Offset vertical radar profiling. Lead. Edge Explor. 22, 1070–1076.

Zhou, H., Sato, M., 2000. Application of vertical radar profiling technique to Sendai Castle. Geophysics 65, 533–539.